RSC Advances

RSC Advances

PAPER

Novel synthesis process for solar light active porous carbon doped CuO nanoribbon and its photocatalytical application for the degradation of organic dye

M. M. Hossain,[a] H. Shima,[b] Md. A. Islam,[c] M. Hasan[d] and M. Lee[d]*

A simple, one step novel solution process was developed for the synthesis of carbon doped CuO (C-CuO) nanoribbons without the use of a catalyst, template, substrate, or costly instrumentation at room temperature. The precursor materials used were converted to C-CuO nanoribbons in ethanol (95%) at high concentrations (4.37mg/ml) as a colloidal solution with very high dispersion stability. The simplicity, reaction time, production cost, production yield, and environmental friendliness of this process makes it suitable for the large scale industrial production of C-CuO nanoribbons. The prepared nanoribbon is also separable and re-dispersible in other organic solvents. The dispersibility in multiple solvent highlights its versatility as a platform to deposit other nanomaterials on its surface in organic media to improve its additional properties as a candidate for other applications. Three dimensional surface morphology was characterized and it suggested the prepared C-CuO nanoribbon was highly porous. Free standing C-CuO nanoribbon films were also prepared using the simple process. The prepared film of porous C-CuO nanoribbon showed excellent light absorption capability in the range of visible to near-IR light with higher intensity. The superior light absorption properties of the C-CuO nanoribbons were utilized as a photocatalyst to decompose organic dye in visible light. The degradation of organic dye (96.64%), recycling performance (93.94%), recycle number (24), and degradation time (120) highlight its potential as a very good photocatalyst.

1.Introduction

Due to the effective transport of electrons and excitons through the smallest length, one-dimensional (1D) semiconductor and metal nanomaterials are reflected the crucial structural constituents of electronic, magnetic and photonic devices causing of their characteristic anisotropy. Their unique properties can be harnessed for the design and fabrication of nanosensors,[1,2] switches,[2] nanolasers,[3] and transistors.[4] Many possible applications of 1D nanomaterials require the formation of well-aligned arrays to accentuate the anisotropy and satisfy the criteria of device design. Copper oxide semiconductor ID materials, such as CuO nanowires (or

nanoribbons), have attracted tremendous attention because of their wide range of applications, such as bioanodes,[5] CO oxidation,[6] supercapacitors,[7] hydrogen production by water reduction,[8,9] H_2O_2 degradation,[10] sodium ion battery,[11] and photon sensing.[12] On the other hand, in most cases, a catalyst, substrate, template, high temperatures, and multiple chemicals and steps were involved in the synthesis of CuO nanoribbons. For example, substrate (copper or silicon, polycarbonate or on other substrate) surfaces[5-6,8-18] are used to grow CuO or Cu_2O or $Cu(OH)_2$ nanowires. In addition, in many cases, the substrates are treated in acid and other solvents for cleaning and to make it active for the growth of nanowires.[5,9,14] High temperatures (400-700°C)[5,6,8,14,16] are used in some cases for the oxidation of the copper substrate but smooth homogeneous nanowires with a high aspect ratio were not achieved.[8,12] The nanowires prepared by these substrate-based processes are applicable to specific applications. To be usable it for flexible applications, the nanowires need to be separated from the substrate surface, which is time consuming, and requires different chemicals and multiple steps.[10] Moreover, there is no procedure reported to separate the grown nanowires from the substrate.[5-6,8-9,11-18] During the separation time, there is high likelihood that the nanowires would be damaged. Indeed, separating nanowires from a substrate is quite difficult. Only very few studies have

[a.] Clean Energy Priority Research Center and School of Chemical Engineering, Yeungnam University, Gyeongsan 712-749, Republic of Korea
[b.] Bioactive Material Sciences, Chonbuk National University, Jeonju 561-756, Republic of Korea
[c.] Department of Pharmacy, Atish Dipankar University of Science & Technology, Banani, Dhaka 1213, Bangladesh and Bioactive Material Sciences, Chonbuk National University, Jeonju 561-756, Republic of Korea
[d.] School of Chemical Engineering, Yeungnam University, Gyeongsan 712-749, Republic of Korea
*Corresponding author email: mynlee@ynu.ac.kr
See DOI: 10.1039/x0xx00000x

been conducted to prepare substrate free CuO nanoribbons in solution over the past few years. Among them, only two processes were considered to be important flexible processes to fabricate well-defined smooth copper oxide nanowires[19,20] in solution. Among these two process, one method requires relatively high temperatures (140-250˚C), reductants (2,5-dimethoxyaniline or o-anisidine or pyrrole), multiple step reactions, and a long time (10-15h) to synthesis CuO nanowires.[19] The reductant has another problem regarding its polymerization in the CuO nanowire solution during the synthesis process. The produced polymer is deposited on the nanowire surfaces as an outer shell layer, which has some negative impact depending on the type of application. For example, in some cases, other conducting or semiconducting metals or metal oxides may be required for direct deposition on the synthesized CuO nanowire surfaces to improve its electrical, optical and electrochemical properties. On the other hand, the polymer works as a deposition barrier for the direct deposition of other materials on the CuO nanowire surfaces because it works as a shell layer. Furthermore, the prepared nanowire should be dispersed in the solution of the other materials to be usable as a platform for the deposition of other nanoparticles in solution. The polymer deposited CuO nanoribbon is not dispersed easily in organic solvents. In another process,[20] polyethylene glycol is used as a surfactant, NaOH is used as a catalyst and hydrazine hydrate ($N_2H_4.H_2O$) is used as a reducing agent for the synthesis of CuO nanowires from $Cu(OH)_2$. Actually, this process is comparatively good but requires multiple steps, which takes time, and needs multiple reagents that leaves impurities in the CuO matrix, environmental pollution and high production cost. Therefore, none of the processes are usable as a low cost novel process for the synthesis of versatile CuO nanoribbons on a large scale. In fact, the novelty of a material depends on its versatility, dispersible capability in other solvents at high concentrations and its simple synthesis process, which should be free from any barrier, such as substrate dependency and complexity.

In this study, carbon doped CuO (C-CuO) nanoribbons were prepared using a single step, catalyst free, low cost, and facile process that allows the large scale industrial production of C-CuO nanoribbons without the assistance of any substrate at room temperature. The prepared nanoribbons showed a very low thickness (2.5-4.0 nm) and narrow (1.31 eV) band gap. Free standing C-CuO nanoribbon films were also prepared using a very simple drop drying process from the as-prepared C-CuO nanoribbon solution without the use of any further instrument, solvent and techniques. This is the first time that substrate free CuO nanoribbon were synthesized in a solution process that can allow industrial scale production. The C-CuO nanoribbons showed excellent visible to near-IR light (400-1665 nm) absorption capability. They were also used as a photocatalyst under sunlight to decompose an organic dye. The photocatalytic degradation and recycling performance highlight it as a very good photocatalyst that is stable against photo-corrosion under sunlight to decompose the organic dye, methylene blue (MB).

2. Experimental work

2.1 Chemicals and Instruments

Chemicals: Copper (11) acetate (98%, Sigma Aldrich), ethanol (absolute, 99.8%, Sigma Aldrich), and ethanol (95%, Duksan, Korea).

Instrument: Structural characterization was conducted using a field emission scanning electron microscopy (FESEM, Nova, S-4800, Hitachi, Japan) and (FE-TEM, TECHNAI G2 F2O S-TWIN, FEI Company, USA). Spectroscopic and crystallographic characterization was done by Raman spectroscopy (HORIBA JOBIN YVON, Lab RAM HR, Laser 514.54 nm, USA) and X-ray diffraction (XRD, thin film, MPD, PANalytical). The optical properties were measured by ultraviolet/visible/near infrared (UV/VIS/NIR, Cary-5000, Agilent) spectroscopy.

2.2 C-CuO nanoribbon

400 mg of copper acetate was taken in a glass vial containing 40 ml ethanol (95%, general grade). Bath sonication was performed at room temperature to achieve dissolution. The prepared clear 10mg/mL solution (Fig. 1a, Scheme A) of copper acetate was further bath sonicated continuously to obtain highly concentrated light blue color C-CuO nanoribbons (Fig. 1b, Scheme A) from a clear teal (deep blue-green) colored solution (Fig. 1a). Generally, it took 2h to produce the complete C-CuO nanoribbons from the copper acetate solution. All the C-CuO nanoribbons were floating in ethanol and were well dispersed. A similar experiment was conducted using pure ethanol (absolute, 99.8%, Scheme B) as a solvent for copper acetate to obtain a highly concentrated light blue color solution but no color change was found (Fig. 1f, Scheme B). Therefore, sonication was also continued for up to 12 h, but no variation in color was observed and no reaction was happened. This shows that C-CuO nanoribbon is not prepared in pure ethanol.

2.3 Free standing C-CuO nanoribbon film

A highly concentrated light blue colored colloid of C-CuO nanoribbons (Fig. 1b) was poured onto white paper (writing paper) and spread out homogenously by slightly shaking the paper. The paper was allowed to dry for 1 h at room temperature (25°C). For quick drying, some tissue paper can be placed under the writing paper, which can decrease the drying time by quickly soaking the ethanol solvent. After drying, the C-CuO nanoribbon film layer deposited on paper (Fig. 1c) was peeled easily by folding the supporting paper in the outward direction (Fig. 1d). The peeled free standing film was further dried at 80°C for 2 h to evaporate the remaining water and ethanol from the film.

2.4 Photocatalytic experiments

The as-prepared C-CuO nanoribbon solution of ethanol (4.37 mg/mL) was centrifuged at 10000 rpm for 1 h and the bottom solution was collected. The resulting bottom solution was diluted to 10 mg/mL and 13 mL, 130 mg, was added to 100 mL of a 7.9 $\times 10^{-4}$ M MB solution in water. The solution was sonicated for 5 min in the dark and settled for 2 h to achieve adsorption and desorption equilibrium. The photocatalytic

degradation of MB was carried out at ambient conditions under direct sunlight, from 10 am to 12 pm. The outside temperature was 28 to 35 °C. A UV light cutoff filter at 420 nm was used over the reaction bottle to block the UV light participation in the photocatalysis reaction. The mixture was sampled at 20 min intervals from under the cutoff filter glass continuously and centrifuged for 10 min in the dark place to discard any sediment. The UV/VIS absorption spectra of all the photocatalysis samples collected at different times were taken. The recycling performance of the C-CuO nanoribbons was measured by collecting the precipitate of the centrifuged products, washing with DI water, drying, and using directly to assess the recycling performance for up to 24 cycles.

3. Result and Discussion

3.1 C-CuO nanoribbon synthesis mechanism

As per the experimental part of synthesis, general grade alcohol (95%) was useful to synthesis C-CuO nanoribbon (reaction 2) and absolute alcohol was not useful for C-CuO

the proton at its O site of OH group. Finally, the product C-CuO nanoribbon (**F**) is produced from product Cu-2 by dehydration shown in last step (**F**) of reaction (4). Here, also, positive charge alcohol attached with acetate ion by its CH_2 carbon by losing one molecule water.

3.2 Characterization of C-CuO nanoribbon

The prepared highly concentrated light blue color C-CuO product in ethanol was placed on silicon wafer and dried to take the SEM and AFM images. SEM (Fig. 2a) revealed a large number of ribbon-shaped C-CuO material on the silicon wafer. High resolution SEM (Fig. 2b) of the C-CuO materials showed a clearly smooth ribbon like shape. Fig. 2a shows average length of C-CuO nanoribbon about 5 µm. Fig. (2b, c) express average width 150 nm. So, average aspect ratio (length:width) of C-CuO nanoribbon is 100:3. TEM (Fig. 2c) also exhibited clearly smooth C-CuO nanoribbons. The high resolution TEM image (Fig. 2d) taken from the rectangular area of Fig. 2c revealed some crystalline parts of the C-CuO nanoribbon. AFM images
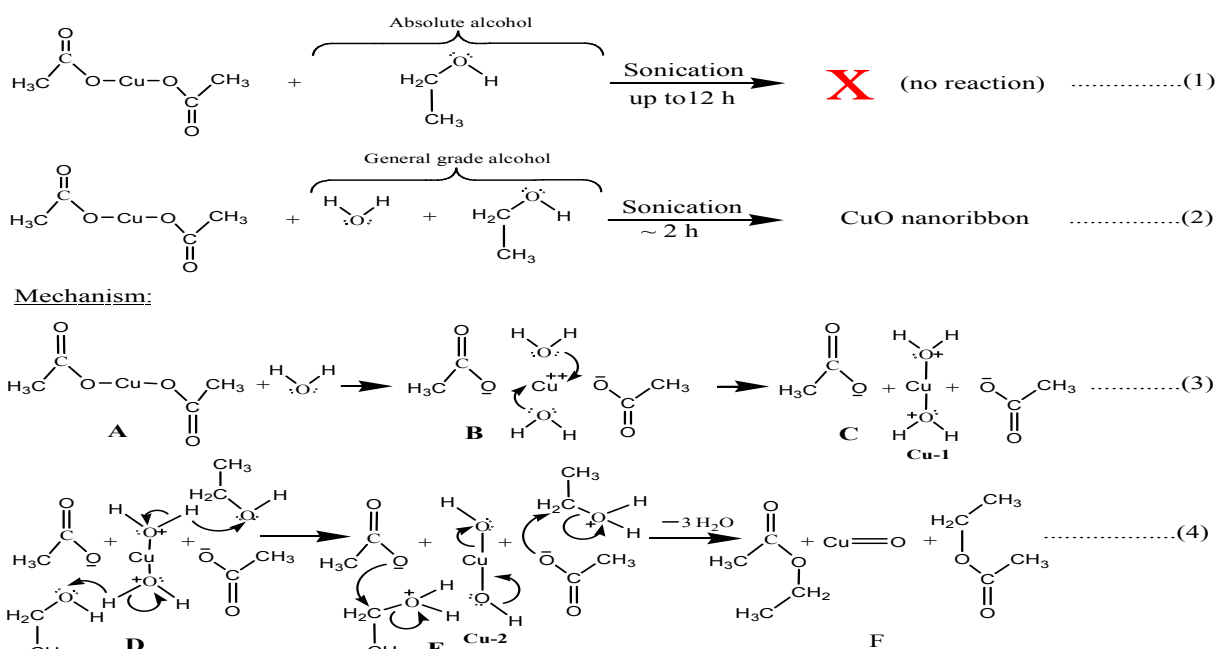
nanoribbon preparation (reaction 1). Usually in general grade alcohol has water (H_2O) and absolute alcohol has no water. Since, general grade alcohol was effective to prepare C-CuO nanoribbon, hence, possibly, the H_2O molecule in alcohol (95%) played significant role for C-CuO nanoribbon synthesis. On the basis of this practical observation, we proposed a reaction mechanism which shows how can water (H_2O) molecule played important role for C-CuO nanoribbon synthesis. Reaction (2) shows sonication of $Cu(CH_3COO)_2$ solution in CH_3CH_2OH + H_2O. Firstly $Cu(CH_3COO)_2$ salt is dissolved (reaction 3) in H_2O of the alcohol (general grade, CH_3CH_2OH + H_2O) as CH_3COO^- and Cu^{++} ion (**B**), in which Cu^{++} ion is surrounded by H_2O molecules (**B**) and produced the product Cu-1. After that, Cu-1 produces Cu-2 product by losing two protons (**D,** reaction 4) and alcohol produces positive charge $^+OH_2$ group (**E,** reaction 4) from OH group by capturing

(Fig. 2e) were taken to confirm the ribbon shaped C-CuO and its thickness, which revealed a smooth ribbon shaped structure. Fig. 2(f, g) shows that ribbons-1 and 2 has a thickness of 3 and 2.5 nm, respectively. Ribbon-2 was thicker (4 nm) at the solid line arrow mark position due to the downward direction bending of the supporting ribbon-1. If ribbon-2 is considered the front side ribbon, the supporting ribbon would be ribbon-1 (marked by dotted arrow). Ribbon-2 resides on ribbon-1 and ribbon-1 resides on ribbon-3, which is clearly seen in the 3D AFM image (Fig. 3b). The AFM image, Fig. 2e, is shown in Fig. 3a. Its corresponding 3D image is also shown in Fig. 3b to exhibit 3D morphology of C-CuO nanoribbon. The 3D image (Fig. 3b) clearly reveals a ribbon shaped morphology and its assembly pattern. The image also expresses a well decorated rough surface (climax) in every nanoribbon. High resolution AFM images (Fig. 3c and Fig. 3d)

from the dotted large and small rectangular area, respectively, were taken to better understand the crest pattern of the CuO nanoparticles in the ribbon. Both images displayed a porous morphology and well organized arrangement of CuO nanoparticles in the ribbon. High resolution 3D AFM (Fig. 3e) showed the real view of the porous morphology of ribbon. For instant, AFM image, Fig. 3c, clearly showing a lot of pore available in the C-CuO nanoribbon. Pores were clearly marked in high resolution C-CuO nanoribbon AFM image (Fig. 3d) and in 3D AFM image (Fig. 3e) by round dotted circles. The total area of the Fig. 3d is 180 nm x 200 nm and total number pores were around 11. Pore sizes were also measured from the Fig. 3d and 3e, and it were about 20-50 nm. Additionally, AFM image, Fig. 3d, was converted to curve (Fig. 3g), which shows clearly the pore diameter. To clearly identify, three lines were drawn along peaks direction and it were relocated to the Fig. 3h. Fig. 3h reveals pore initiation diameter and actual pore size is about 40 nm. In addition, the AFM palette setting image (Fig. 3f) taken from Fig. 3d showed the crest, rising and falling action of the CuO nanoparticles in a ribbon. One crest positon was marked with an arrow in Fig. 3d and this same position is shown in Fig. 3f by arrow marking. A few pore positions were marked by i, ii, iii, iv, v, and vi in Fig. 3f, and its corresponding position is also shown in Fig. 3d.

All the XRD peaks (Fig. 4a) were assigned to the monoclinic phase of CuO oxide, which is in good agreement with the JCPDS (05-0661).[21,22] The major peaks at 35.45 and 37.73° 2θ were indexed as the (–111)/(002) and (111)/(200) planes, respectively.[22] A broad band peak at the 24.81 position was observed, which is the characteristic peak of the 002 plane of carbon materials. This peak indicated that carbon is available in the C-CuO nanoribbon. During the synthesis process, carbon was incorporated in the nanoribbon structure and possibly played a significant role in the formation of the nanoribbon structure. The pristine graphitic carbon peak is generally found at ~25° 2θ, but in this case, it was found at a higher d-spacing positon. The higher d-spacing can have two explanations. One is the low crystalline carbon and another is the interactions of CuO nanoparticles with carbon.

The Cu2p XP spectrum (Fig. 4b) was taken to examine the valence of Cu, its defects and other properties in the C-CuO nanoribbons. Two distinctive peaks with binding energies of 933.88 eV and 954.18 eV for Cu $2p_{3/2}$ and Cu $2p_{1/2}$, respectively, were observed and corresponded to Cu(II) oxide.[23] Two new peaks as satellite peaks at a binding energies of 942.38 and 962.38 eV were observed.[24] The deconvoluted curve of the core level C1s XP spectra (Fig. 4c) revealed several components at 284.61, 285.97, 286.66, and 288.68, which were assigned to the C=C bond of sp^2 carbon, C-C bond for sp^3 amorphous carbon, C-O-C, and (C=O)O, respectively.[25] From these C1s core level peaks, it was found that the C-CuO nanoribbon has carbon containing different functional groups. This might have been chemical bonded to Cu of CuO, which was also predicted by XRD. The peak positons were shifted slightly due to the interaction with CuO or because of chemical bonding. The very low energy position peak, 288.8 eV, was

assigned to the chemical bond between Cu and C, such as Cu-C.[26,27] The O1s peaks (Fig. 4d) were de-convoluted into two peaks located at 530.49 and 531.82 eV, which are associated with the lattice oxygen of CuO and surface-adsorbed oxygen species (OH) groups, respectively.[28] The O1s original curve and the summation curve of the deconvoluted curves were matched together, which are also shown in Fig. 4d (the upside curves). The peaks were shifted slightly owing to the *in-situ* incorporation of carbon in the nanoribbon structure of CuO.

For further investigation, the Raman spectra of C-CuO nanoribbon were also examined. The Raman spectra (Fig. 4e) revealed two peaks located at 296.85 (Ag) and 615.06 (Bg) cm^{-1}, which are characteristic of CuO.[7] The peaks at 405.19 and 484.42 cm^{-1} are accountable for $4\Gamma^-_{12}$ and Γ^+_{25} peaks,[29] respectively, of Cu_2O. These (405.19 and 484.42 cm^{-1}) peaks showed that the prepared C-CuO nanoribbon has few Cu_2O oxides. Both of these ($4\Gamma^-_{12}$ and Γ^+_{25}) these peaks were shifted slightly to the lower frequency position due to carbon incorporation with the CuO nanoribbon. The peaks at 1345.9, 1574.1 and 2678.1 cm^{-1} are the characteristic D, G and 2D band peaks of carbon. The D band at the 1345.9 position indicates that defects are available in the carbon structure, which might explain some of the functional groups in carbon, which was also confirmed by the XPS C1s core level spectrum (Fig. 4c).

3.3 Dispersion capability

We separated C-CuO nanoribbon from ethanol solvent by centrifugation and then we re-disperse it in *N-methyl*-2-pyrrolidone (NMP) and Dimethylformide (DMF) solvent separately to check dispersion capability and stability. In both of the solvent C-CuO nanoribbon showed very high dispersion capability (4.5 mg/mL) and stability as like ethanol solvent (4.37mg/mL). So, this very high concentration solution can be usable for deposition of any metal nanoparticles or semiconductor nanoparticles on C-CuO nanoribbon surfaces by flexible organic media. We also checked deposition capabilities of very high concentration colloid on other substrate surfaces (i.e. quartz glass, silicon wafer, FTO, ITO, mica, etc.) to be usable as a candidate of other application. It showed good deposition or self-assemble capabilities on the above mentioned substrate surfaces. Additionally, for making polymer-semiconductor composite, the homogeneous dispersion of semiconductor with high concentration in organic solvent is very important. Because, in-situ polymerization can be done in this high concentration homogeneous solution and semiconductor can be well dispersed in polymer matrix with high interaction to improve polymer's optical and mechanical property. So, our C-CuO nanoribbon colloidal solution (4.37 mg/mL) shows high possibility as a filler to make polymer-CuO composite.

3.4 C-CuO nanoribbon film and its optical properties

To measure the light absorbance properties of the C-CuO nanoribbon, a C-CuO nanoribbon film (Fig. 5a) was prepared using a very simple process without using special instrumentation, as per the experimental section. Fig. 5b

shows a low resolution SEM image of the free standing film. To clearly display the pattern and structure of the small area of the free standing film, Fig. 5c was taken from the rectangular dotted area of Fig. 5b. Fig. 5d was also taken from the rectangular dotted area of Fig. 5c. Many C-CuO ribbons were observed in Fig. 5d. Fig. (5e, f) show high resolution SEM images of the rectangular marked area of Fig. 5d and Fig. 5e, respectively. This (Fig. 5e, f) showed a clearer view of the C-CuO nanoribbons.

The C-CuO nanoribbon film was used to take a UV-Visible near-IR spectrum (Fig. 6a). The film exhibited good light absorption properties from the visible to near IR region (400-1675 nm). This light absorption intensity and range (400-1675 nm) of the C-CuO nanoribbon film is higher than that of the other nanoribbon/nanowire or nanoparticles composites [19,30-35] of CuO or Cu_2O. A high intensity broad band absorption peak was observed at 625 nm. The band gap of the as-prepared C-CuO nanoribbon can be calculated (Fig. 6b) using Equation (1),[36] where E_g is the band gap energy, hv is the photo energy, A is the relevant transition characteristic parameter, and ɣ =1/2 or 2 for a direct or indirect transition between the valence band and conduction band, respectively.

$$\alpha hv = A(hv - E_g)^\curlyvee \dots\dots\dots\dots. (1)$$

Considering the direct transition, Fig. 6b shows $(\alpha hv)^2$ vs. photon energy (eV) curve[37,38]; a direct band gap of 1.31 eV was measured for the C-CuO nanoribbon. Cu participated in chemical bonding (i.e. Cu-O-C, Cu-C),[39] as with other metal oxides,[37,40] by the functional group of carbon at the defect site. Possibly, a defect was created in the CuO matrix due to the direct (Cu-C) or indirect (Cu-O-C) chemical bonding of carbon with Cu and eventually the band gap decreased. The narrower band gap of the C-CuO nanoribbon can also explain the greater light absorption at the longer wavelength.

3.5 Photocatalytic performance
Fig. 6c shows the MB decomposition in presence of C-CuO nanoribbon for 0, 20, 40, 60, 80, 100, and 120 min photocatalytic reaction under direct sunlight in outdoor environment. UV cut off filter glass (65CGA-420 CG495, 50% T point at 420.70 nm, Newport) at 420 nm was used over the reaction vessel in outdoor environment to block the UV light from natural sunlight in the photocatalytic reaction. The decomposition rate (Fig. 6d) of MB in the presence of C-CuO occurred sharply at a 20 min reaction. On the other hand, the degradation rate was comparatively slower in the case of 40 to 120 min reactions. The degradation rate of MB was calculated using Equation (2).[38,41,42] Here, η = degradation rate, A_0 = Absorbance at zero min decomposition time and A_t = is the absorbance at the decomposition reaction time, t.

$$\eta = \frac{A_0 - A_t}{A_0} \times 100 \dots\dots\dots\dots.. (2)$$

Fig. 6e also shows the absorbance curve of recycling performance of C-CuO nanoribbon for up to 24 cycles. Every photocatalysis reaction was done for 120 min in the presence C-CuO. The C-CuO nanoribbons were collected by filtration followed by washing and drying. After separation of the C-CuO nanoribbon by filtration, the filtered MB solution was used to take the UV-Visible spectra to measure the absorbance to calculate the degradation rate. The absorbance curve of photo-catalytically degraded MB solution of the 1st, 6th, 12th, 18th and 24th cycles product (Fig. 6e) were used directly to calculate degradation rate in percentage. The degradation rate of the 1st, 6th, 12th, 18th and 24th cycles MB solution in presence of C-CuO nanoribbon were 98.1, 96.3, 95.9, 95.6 and 95.4% (Fig. 6f). Additionally, for the measurement of self-degradation of MB, a control reaction was done without photocatalyst and this curve was shown Fig. 6c. From the absorbance of that curve self-degradation (1.46%) was calculated by the equation (2). So, Actual degradation by C-CuO nanoribbon was calculated by deduction of self-degradation (1.46%) from the first cycle's product degradation. As for example, degradation of first cycles and control reaction (self-degradation) were 98.1% and 1.46%, respectively. So, Actual degradation was 96.64% (98.1-1.46= 96.64%). Similarly, the actual degradation rates of MB at 24th cycle was 93.94%. This means only a 2.7% (96.64-93.94=2.7%) decrease in the degradation rate after 24 recycles. The very high actual degradation rate (93.94%) of the C-CuO nanoribbons recycled 24 times suggests that the prepared nanoribbons are highly stable against photo corrosion. This recycling performance curve (Fig. 6f) clearly showed a rapid decrease in degradation in the first 6 cycles that became slower at 6-12, 12-18 and 18-24 cycles. The excellent photocatalysis performance is achieved not for a single reason, but the combined narrow band gap of the C-CuO nanoribbon, carbon participation as a platform of electron transfer in C-CuO nanoribbon, oxygen vacancy defect of C-CuO nanoribbon and the porous structure of C-CuO nanoribbon. As for example, carbon materials (carbon nanosheet or graphene or other forms of carbon) can improve the electrical conductivity of semi-conductive materials. Additionally, carbon materials can play a significant role to improve photoactivity of photocatalyst as a photoelectron reservoir.[43] Due to the high electrical conductivity of carbon materials, it can receive electron so fast from the valence band of semiconductor to the carbon and enhancing separation efficiency of photo-generated electron-hole pairs by working as inhibitor of recombination.[43] Since, the interface of C-CuO system was strongly bound by chemical bond which were described by XPS analysis (Fig. 4c, d), so, migration electron to carbon surface from the CuO nanoribbon was more convenient through the good interfacial interaction or by the chemical bond bridge at interface. As a result, the life time of photo-generated charge carriers was improved by decreasing recombination.[43,44,45,46,47] It was also investigated that carbon materials enhance the dye adsorption capability of semiconductor as composite and this more dye adsorption behavior is helpful for more dye degradation.[44,47] Furthermore, 2D carbon materials significantly improve the light absorption properties semiconductor

materials by controlling band gap[45] which is also crucial for developing photocatalytic performance.

Fig. 7 shows the possible decomposition mechanism of MB with the help C-CuO nanoribbon photocatalyst. When the porous CuO nanoribbon is exposed to sunlight (Fig. 7a), an electron is excited from its valence band (VB) to the conduction band (CB) (Fig. 7b). This photo-excited electron in the conduction band is transferred quickly to the nearest high conductive carbon surface as per above discussion (Fig. 7c) by its chemical bond bridge. Since, CuO is a p-type semiconductor with the valence and conduction band edges at +1.25 V and +0.45 V vs NHE[48] (Fig. 7e). On the other hand, conduction band of carbon materials 0.08 V vs NHE [45, 49,50] (Fig. 7e). So, due to the sunlight irradiation, the electrons are excited from valence band to the conduction of CuO nanoribbon and these excited electron easily transferred to the convenient band position of carbon sheet (Fig. 7e). The photo-excited electron is then used to prepare $O_2^{\bullet-}$ species [47,51,52] (Fig. 7b) in the presence of dissolved oxygen in H_2O on the two dimensional surface of carbon.[47,51,52] The prepared active $O_2^{\bullet-}$ species were used to prepare active $^{\bullet}OH$ free radicals in presence of ^{+}H followed by reaction (6).[47,51,52] Here, ^{+}H is prepared by reaction (5). Then $^{\bullet}OH$ directly attacks the MB dye molecule (Fig. 7b), reaction (8), for degradation.[47,51,52] During the photo-excitation, active $^{\bullet}OH$ free radicals are also prepared from a H_2O molecule, reaction (7), (Fig. 7b) by the reaction with the hole of the VB.[47,51, 52] Here, MB decomposition is achieved by attacking the active $^{\bullet}OH$ (Fig. 7b) at the VB. Recombination of the photo-excited electron from the CB to VB is unlikely due to the quick electron transfer to the adjacent high conductive carbon surface. The high conductive carbons can quickly receive this photo-excited electron by its possible chemical bonding bridge with CuO (i.e. Cu-C or Cu-O-C or Cu-O-O-C), as shown in Fig. 7c. Therefore, carbon works as an inhibitor of recombination and enhances the decomposition rate of photocatalysis reaction, which is very important for the photocatalysis reaction. The carbon sheet existence was shown by HRTEM image in Fig. 7d. The yellow marked arrows clearly indicates few layer carbon sheet edges. The C-CuO nanoribbon edge was shown by red dotted line.

$$H_2O \rightleftharpoons {}^{+}H + {}^{-}OH \quad \text{...} (5)$$

Conduction band reaction:

$$O_2 + {}^{\ominus}e \rightarrow O_2^{\bullet-} \xrightarrow{{}^{+}H} HO_2^{\bullet} \xrightarrow[-O_2]{HO_2^{\bullet}} H_2O_2 \rightarrow {}^{-}OH + {}^{\bullet}OH \quad \text{.......} (6)$$
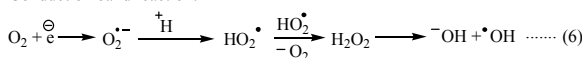
Valence band reaction:

$$\oplus(\text{hole}) + {}^{-}OH \rightarrow {}^{+}H + {}^{\bullet}OH \quad \text{...} (7)$$
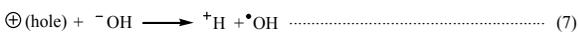
Decomposition of MB by active ${}^{\bullet}OH$:

$$MB + {}^{\bullet}OH \rightarrow CO_2 + H_2O + \text{.........} \quad \text{.......................................} (8)$$

Conclusions

Porous C-CuO nanoribbons were prepared in solution using a novel facile route without a substrate. The substrate is a significant barrier to separating the prepared C-CuO nanoribbons from the substrate surface for dispersion in solution for other application purposes. This substrate free process is performed without a catalyst, template and costly instrumentation at room temperature. Furthermore, the use of precursor materials and solvent are of general grade and lower priced. The dispersion concentration (4.37mg/ml) of the C-CuO nanoribbon in ethanol solvent was also measured, which is also a very high concentration and shows very higher dispersion stability. Because the prepared nanoribbon can be dispersed in other organic solvents, so, the prepared C-CuO can be usable in other organic medium for other materials deposition on it. The light absorption capabilities (400-1665 nm) with high intensity, dye degradation performance 96.6% (by deducting self-degradation), utilization direct sunlight as light source and photo-stability against photo-corrosion up to 24 cycles indicated Cu-CuO nanoribbon is the excellent photocatalyst in outdoor environment under direct sunlight. Considering the simplicity, reaction time, production cost, production yield, environment friendliness, and photocatalytic performance, this process provides the best opportunity for the large scale industrial production of C-CuO nanoribbon.

References

1 Y. Cui, Q. Q. Wei, H. K. Park and C. M. Lieber, *Science,* 2001, **293**, 1289-1292.
2 F. Favier, F. C. Walter, M. P. Zach, T. Benter and R. M. Penner, *Science,* 2001, **293**, 2227-2231.
3 M. H. Huang, S. Mao, H. Feick, H. Q. Yan, Y. Y. Wu, H. Kind, E. Weber, R. Russo and P. D. Yang, *Science,* 2001, **292**, 1897-1899.
4 L. J. Lauhon, M. S. Gudiksen, D. L. Wang and C. M. Lieber, *Nature,* 2002*,* **420**, 57-61.
5 F. Qian, G. Wang and Y. Li, *Nano Lett*., **2010**, **10**, 4686–4691.
6 Y. Feng and X. Zheng, *Nano Lett.,* 2010, **10**, 4762–4766.
7 Q. Yu, H. Huang, R. Chen, P. Wang, H. Yang, M. Gao, X. Peng and Z. Ye, *Nanoscale,* 2012, **4**, 2613–2620.
8 Z. Zhang, R. Dua, L. Zhang, H. Zhu, H. Zhang and P. Wang, *ACS Nano,* 2013, **7**, 1709–1717.
9 A. Kargar, Y. Jing, S. J. Kim, C. T. Riley, X. Pan and D. Wang, *ACS Nano,* 2013, **7**, 11112–11120.
10 H. Zhou and S. S. Wong, *ACS Nano,* 2008, **2**, 944–958.
11 S. Yuan, X. Huang, D. Ma, H. Wang, F. Meng and X. Zhang, *Adv. Mater*., 2014, **26**, 2273–2279.
12 S. Sahoo, S. Husale, B. Colwill, T. Lu, S. Nayak and P. M. Ajayan, *ACS Nano,* 2009, **3**, 3935–3944.
13 X. Wen, W. Zhang, S. Yang, Z. R. Dai and Z. L. Wang, *Nano Lett.,* 2002, **2**, 1397-1401.
14 X. Jiang, T. Herricks and Y. Xia, *Nano Lett.,* 2002, **2**, 1333-1338.
15 Y. Qin, Y. Yang, R. Scholz, E. Pippel, X. Lu and M. Knez, *Nano Lett.,* 2011, **11**, 2503–2509.
16 Y. Feng, I. S. Cho, P. M. Rao, L. Cai and X. Zheng, *Nano Lett.,* 2013, **13**, 855–860.

17 Y. Zhou, S. Kamiya, H. Minamikawa and T. Shimizu, *Adv. Mater.,* 2007, **19**, 4194–4197.
18 B. Sciacca, S. A. Mann, F. D. Tichelaar, H. W. Zandbergen, M. A. V. Huis and E. C. Garnett, *Nano Lett.,* 2014**, 14**, 5891−5898.
19 Z. Zhang, R. Dua, L. Zhang, H. Zhu, H. Zhang and P. Wang, *ACS Nano,* 2013, **7**, 1709–1717.
20 W. Wang, G. Wang, X. Wang, Y. Zhan, Y. Liu and C. Zheng, *Adv. Mater.,* 2002, **14**, 67-69.
21 B. Liu and H. C. Zeng, *J. Am. Chem. Soc.,* 2004, **126**, 8124-8125.
22 R. Gusain and O. P. Khatri, *J. Mater. Chem. A,* 2013, **1**, 5612–5619.
23 K. Y. Lee, H. Hwang, D. Shin, W. Choi, *J. Mater. Chem. A,* 2015, **3**, 5457–5466.
24 S. Hsieh, P.-Y. Lin and L.-Ya. Chu, *J. Phys. Chem. C,* 2014, **118**, 12500−12505.
25 C.-C. Teng, C.-C. M. Ma, C.-H. Lu, S.-Y. Yang, S.-H. Lee, M.-C. Hsiao, M.-Y. Yen, K.-C. Chiou and T.-M. Lee, *Carbon*, 2011, **49**, 5107-5116.
26 Y.-P. Zhu, M. Li, Y.-L. Liu, T.-Z. Ren and Z.-Y. Yuan, *J. Phys. Chem. C,* 2014, **118**, 10963-10971.
27 X. Zhou, Y. Li, T. Peng, W. Xie and X. Zhao, *Mater. Lett.,* 2009, **63**, 1747-1749.
28 Z.-J. Zuo, J. Li, P.-D. Han and W. Huang, *J. Phys. Chem. C,* 2014, **118**, 20332–20345.
29 L. Pan, J.-J. Zou, T. Zhang, S. Wang, Z. Li. Wang and X. Zhang, *J. Phys. Chem. C,* 2014, **118**, 16335–16343.
30 X. Qiu, M. Miyauchi, K. Sunada, M. Minoshima, M. Liu, Y. Lu, D. Li, Y. Shimodaira, Y. Hosogi, Y. Kuroda, K. Hashimoto, *ACS Nano,* 2012, **6**, 1609–1618.
31 L. Zhang, D. A. Blom and H. Wang, *Chem. Mater.,* 2011, **23**, 4587–4598.
32 M. T. Qamar, M. Aslam, I. M. I. Ismail, N. Salah and A. Hameed, *ACS Appl. Mater. Interfaces,* 2015, **7**, 8757−8769.
33 H.-Y. Jiang, G. Liu, M. Li, J. Liu, W. Sun, J. Ye and J. Lin, *Applied Catalysis B: Environmental,* 2015, **163**, 267–276.
34 M. D. Susman, Y. Feldman, A. Vaskevich and I. Rubinstein, *ACS Nano,* 2014, **8**, 162–174.
35 G. Yin, M. Nishikawa, Y. Nosaka, N. Srinivasan, D. Atarashi, E. Sakai and M. Miyauchi, *ACS Nano,* 2015, **9**, 2111–2119
36 H. Weidong, Q. Wei, W. Xiaohong and N. Hailong, *Mater. Lett.,* 2007, **61**, 4100-4102.
37 M. Samadi, H. A. Shivaee, M. Zanetti, A. Pourjavadi and A. Moshfesgh, *Journal of Molecular Catalysis A,* 2012, **359**, 42-48.
38 M. M. Hossain, B.-C. Ku and J. R. Hahn, *J. Appl. Surf. Sci.,* 2015, DOI: 10.1016/j.apsusc.2015.01.191

39 B. L. Hurley and R. L. McCreery, *J. Electrochem. Soc.,* 2004, **151**, B252-B259
40 D. I. Son, B. W. Kwon, D. H. Park, W. S. Seo, Y. Yi, B. Angadi, C. L. Lee and W. K. Choi, *Nat. Nanotechnol.,* 2012, **7**, 465-471.
41 L. Xu, G. Zheng, J. Wang, M. Lai, J. Miao, F. Xian, F. Gu and T. Sun, *Mater. Lett.,* 2014, **122**, 1-4.
42 Y. Yan, Z. Zhou, W. Li, Y. Zhu, Y. Cheng, F. Zhao and J. Zhou, *RSC Adv.,* 2014, **4**, 38558-38567.
43 C. Han, M.-Q. Yang, B. Weng and Y.-J. Xu, *Phys. Chem. Chem. Phys.,* 2014, **16**, 16891-16903.
44 Y. Zhang, Z. -R. Tang, X. Fu and Y. –J. Xu, *ACS Nano,* 2010, **4**, 7303-7314
45 C. Han, Z. Chen, N. Zhang, J. C. Colmenares and Y.-J. Xu, *Adv. Funct. Mater.,* 2015, **25**, 221–229
46 M.-Q. Yang, N. Zhang, M. Pagliaro and Y.-J. Xu, *Chem. Soc. Rev.,* 2014, **43**, 8240—8254
47   N. Zhang, M. -Q. Yang, S. Liu, Y. Sun and Y. –J. Xu, *Chem. Rev.,* 2015, **115**, 10307−10377.
48 M. T. Qamar, M. Aslam, I. M. I. Ismail, N. Salah and A. Hameed, *ACS Appl. Mater. Interfaces*, 2015, **7**, 8757–8769.
49 M. -Q. Yang and Yi.-J. Xu, *Phys. Chem. Chem. Phys.,* 2013, **15,** 19102—19118.
50 J. Zhang, J. Yu, M. Jaroniec and J. R. Gong, *Nano Lett.,* 2012, **12**, 4584–4589.
51 A. Houas, H. Lachheb, M. Ksibi, E. Elaloui, C. Guillard, J.-M. Herrmann, *Appl. Catal. B,* 2001, **31**, 145–157.
52 T. S. Natarajan, K. Natarajan, H. C. Bajaj, R. J. Tayade, *J. Nanopart. Res.,* 2013, **15**, 1669

Figure 1
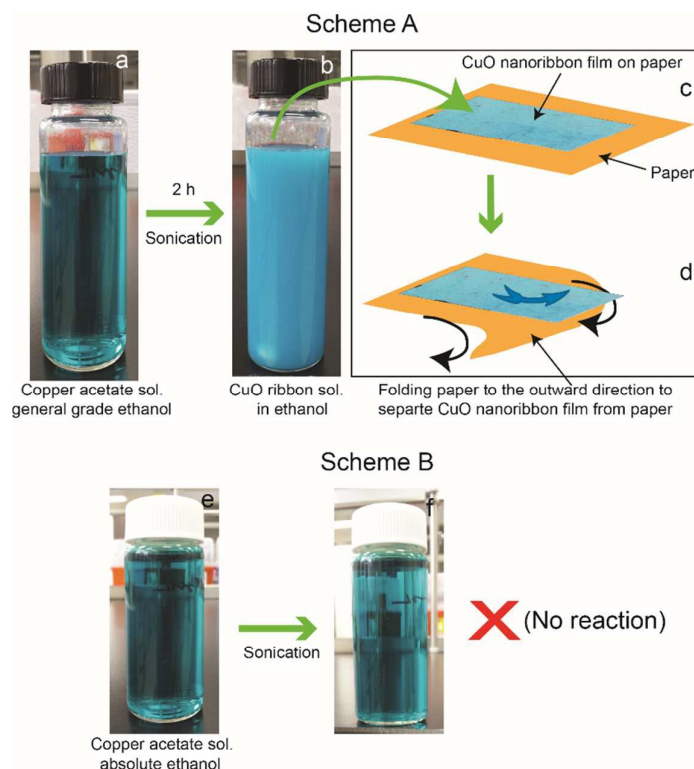
Fig. 1 Scheme A: Schematic diagram of C-CuO nanoribbon and its film preparation by general grade ethanol, a) copper acetate 10 mg/mL solution in general grade ethanol, b) C-CuO nanoribbon solution (4.37 mg/mL) in ethanol, c) C-CuO nanoribbon film prepared on paper, d) C-CuO nanoribbon film separation technique from paper. Scheme B: Schematic diagram showing absolute ethanol is not effective for C-CuO nanoribbon synthesis, e) copper acetate solution in absolute ethanol, f) after 12 h sonication no color change is happened.

Figure 2
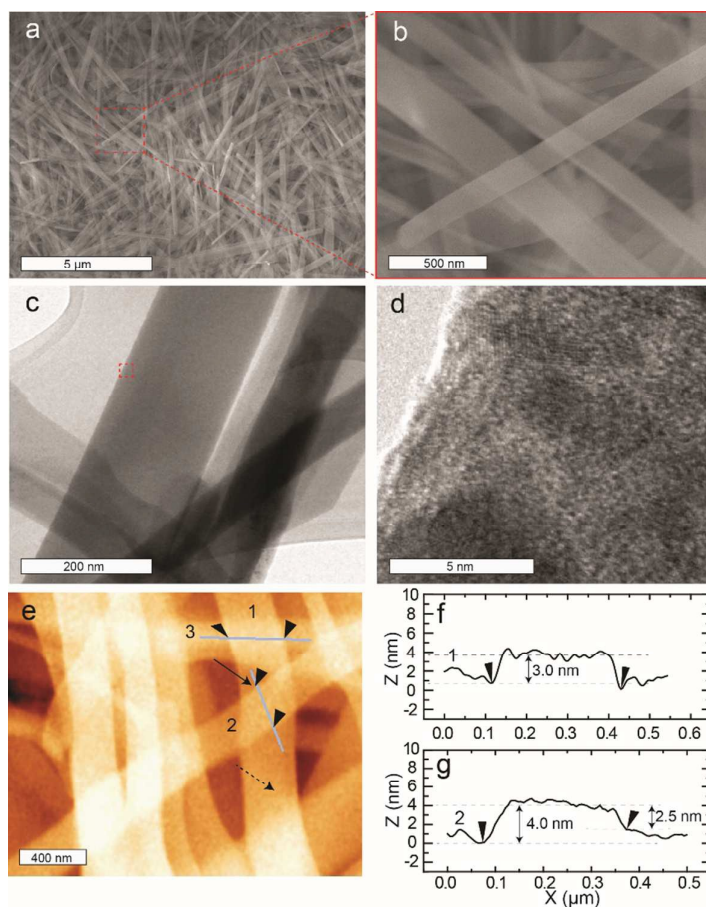
Fig. 2 SEM and AFM images: (a) C–CuO nanoribbon SEM image, (b) high resolution SEM image of C–CuO nanoribbon, (c) TEM image of C–CuO nanoribbon, (d) HR-TEM image of C–CuO nanoribbon, (e) AFM image of C–CuO nanoribbon, (f) thickness of C–CuO nanoribbon-1, and (g) thickness of ribbon-2.

Figure 3
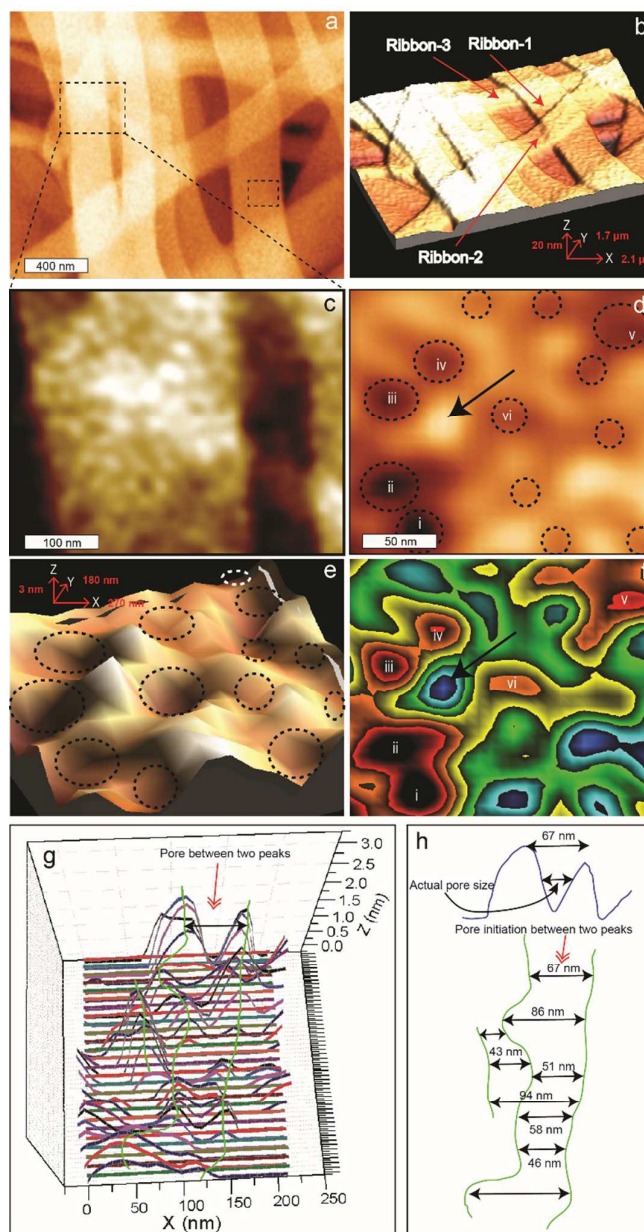
Fig. 3 3D morphology of C-CuO nanoribbon: (a) AFM image of the C-CuO nanoribbon, (b) 3D AFM image of C-CuO nanoribbon taken from Fig. 3a, (c) High resolution AFM image taken from the big rectangular marked area, (d) high resolution AFM image taken from the small rectangular area of Fig. 3a, (e) 3D AFM image of smaller area, (f) AFM palette setting image taken from Fig. 3d, (g) Fig. 3d was converted to curve, (h) drawing ling along the peaks direction in Fig. 3g was shown here separately.

Figure 4
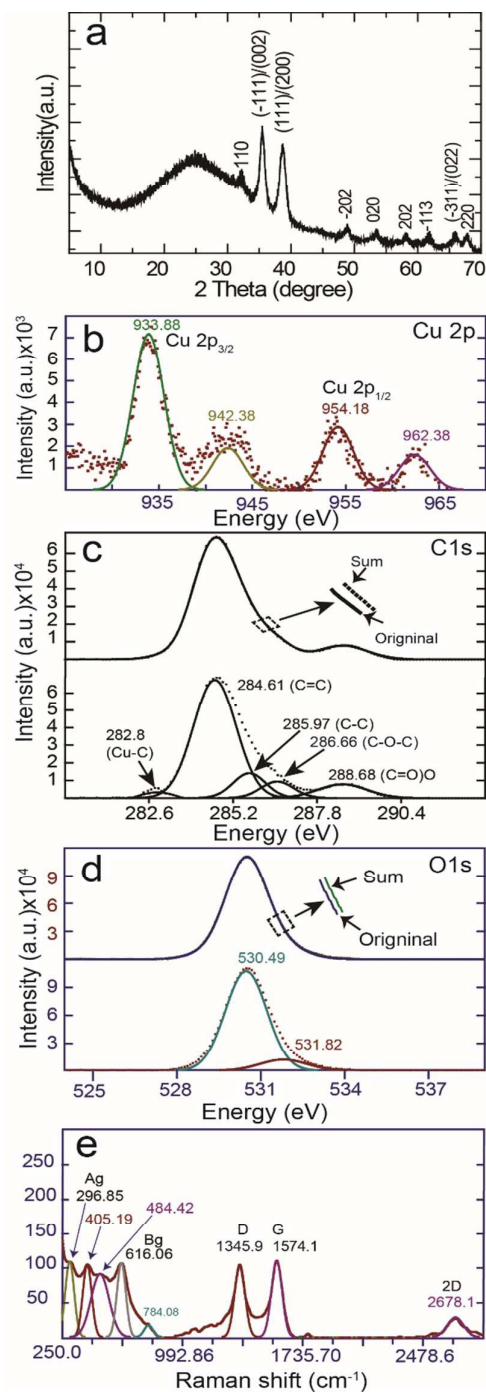
Fig. 4 XRD, XPS and Raman: (a) XRD pattern of C-CuO nanoribbon, (b) Cu 2p XP spectrum of C-CuO nanoribbon, (c) C1s spectrum of C-CuO nanoribbon, (d) C-CuO nanoribbon O1s XP spectrum and (e) Raman spectra of C-CuO nanoribbon.

Figure 5
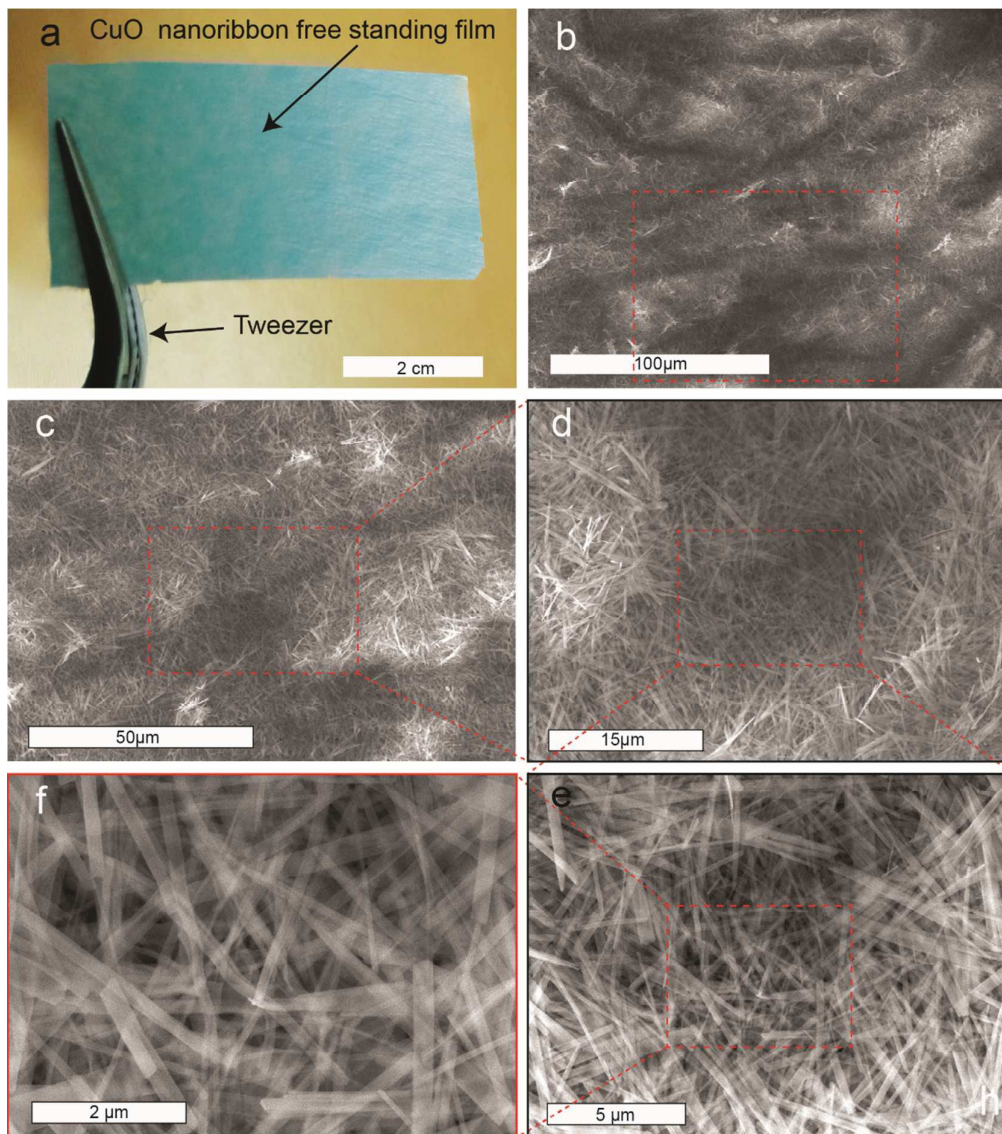
Fig. 5 C–CuO nanoribbon free standing film photograph and SEM image: (a) Photograph of C-CuO nanoribbon free standing film, (b) SEM image of the C-CuO nanoribbon film, (c) SEM image of the C-CuO nanoribbon film taken from the rectangular area of Fig. b, (d) SEM image of the C-CuO nanoribbon film taken from the rectangular area of Fig. c, (e) SEM image of the marked rectangular area of Fig. d, and (f) high resolution SEM image taken from the rectangular area of Fig. e.

Figure 6
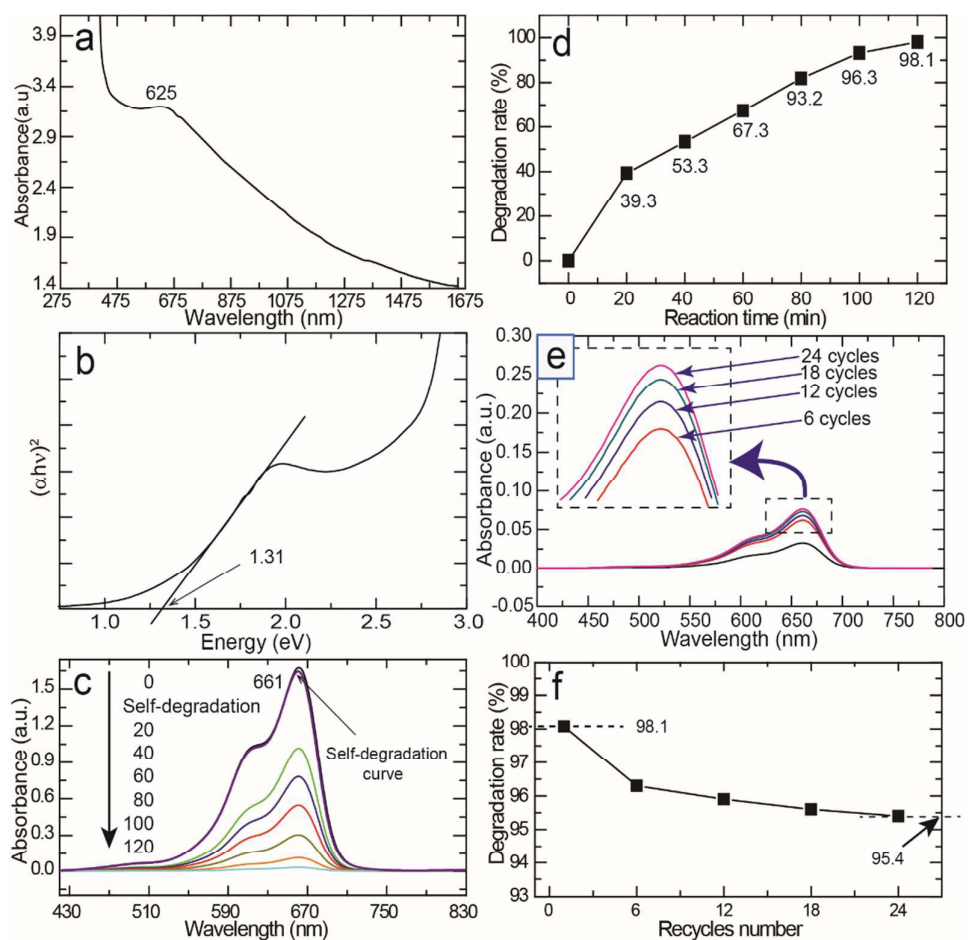
Fig. 6 Light absorption, band gap and photo degradation: (a) UV-Visible-NIR absorbance curve of the C-CuO nanoribbon film, (b) $(\alpha h\nu)^2$ vs. photon energy (eV) curve for calculating the band gap of the C-CuO nanoribbon, (c) photo degradation curves of different degradation times, (d) degradation rate vs. reaction times curve, (e) absorbance curves of photo-degraded MB solution of 6, 12, 18, 24 cycled products and (f) degradation rate vs. recycles number curve.

Figure 7
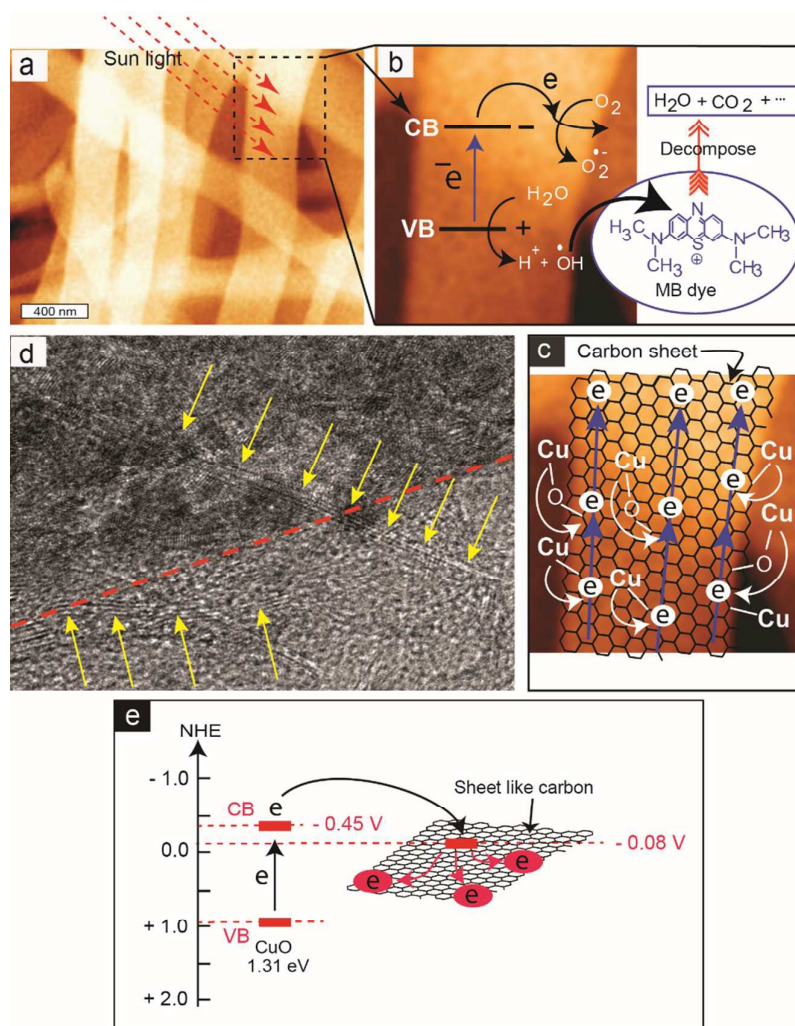
Fig. 7 Photo degradation mechanism: (a) Solar light incident on the C-CuO nanoribbon, (b) electrons are excited from VB to CB and transferred via carbon, and finally producing ˙OH species, which were used to decompose dye, (c) electron transferring to carbon sheet via a chemical bond, (d) HRTEM image of C-CuO nanoribbon in which edge is shown by red dotted line. Upside of the red dotted line is CuO nanoparticles. Yellow arrow indicating few layers carbon sheet edge and (e) Band position of CuO nanoribbon and carbon materials, which shows convenient band for transferring electron to carbon sheet from conduction band of CuO nanoribbon.

76x38mm (300 x 300 DPI)